Generation and evolution of internal waves in the Strait of Gibraltar

A numerical study

The generation and evolution of large amplitude internal waves (LAIWs) in the Strait of Gibraltar is investigated in the framework of a three-dimensional, fully nonlinear, non-hydrostatic numerical model. The model reproduces the mean exchange through the Strait, and it is forced by a realistic tidal barotropic flow for a duration of one tropical month. Modelling efforts focused on the sensitivity of the generation process to the fortnightly tidal signal (neap-spring tides), so far not analyzed, and on the influence of transversal variations of the barotropic flow over Camarinal Sill (CS). Results reveal two distinct kinds of baroclinic response at CS depending on the intensity of tidal forcing. Under moderate forcing, two internal hydraulic jumps are observed in the Strait, one located upstream, which eventually disintegrates in a series of solitary waves propagating to the Alboran Sea, the second one located at the lee side of the sill where flow bifurcation and strong water mixing occur. When the intensity of barotropic tidal flow intensity exceeds a certain threshold, the upstream hydraulic jump is swept downstream where it merges with the one located at the lee side

Jose Carlos Sanchez-Garrido, Gianmaria Sannino, Luca Liberti

Generazione ed evoluzione delle onde interne nello Stretto di Gibilterra. Uno studio numerico

La generazione e l'evoluzione di onde interne di grande ampiezza nello Stretto di Gibilterra è stata analizzata attraverso un modello tridimensionale, non lineare e non idrostatico. Il modello riproduce lo scambio medio attraverso lo stretto ed è forzato con un flusso mareale barotropico realistico per la durata di un mese tropico. Lo strumento modellistico è stato utilizzato per lo studio della sensibilità del processo di generazione alla modulazione del segnale mareale, ad oggi non analizzata, e alla studio del ruolo delle variazioni trasversali del flusso baritropico sopra la sella di Camarinal. I risultati evidenziano la presenza di due tipi di risposta baroclinica a CS che si realizzano a seconda dell'intensità della forzante mareale. Per cicli mareali di intensità moderata si registra la presenza di due risalti idraulici interni nello stretto: uno posto a monte, che finisce per disintegrarsi in una serie di onde solitarie che si propagano nel mare di Alboran, l'altro posto sulla parete di valle della sella dove il flusso si biforca e si realizza un forte mescolamento. Quando l'intensità del flusso barotropico supera un valore di soglia, il risalto collocato a monte viene spinto verso valle dove si unisce col risalto di valle

Jose Carlos Sanchez-Garrido
Dpto Fisica Aplicada II, University of Malaga, Malaga, Spain
Gianmaria Sannino
ENEA, Unità Tecnica Modellistica Energetica Ambientale
Luca Liberti
ISPRA

Introduction

The Strait of Gibraltar (hereinafter SoG) is a very particular place of the World Ocean connecting the Mediterranean Sea and the Atlantic Ocean through a complex bottom topography including a system of sills and narrows (Figure 1a). This circumstance has converted this spot in the focal point of intensive research, mostly involving its mean circulation, traditionally considered an excellent geophysical example of a two-layer exchange flow (Farmer and Armi, 1988; Bryden and Kinder, 1991). The exchange fluctuates at very different time scales, exhibiting tidal, meteorological, seasonal, and interannual variability (Candela et al., 1989). Among all these scales the tidal band is by far the most energetic one. In fact, strong barotropic tidal currents are responsible for the generation of large amplitude internal waves (LAIWs) at Camarinal Sill (CS), the mean sill of the Strait (Richez, 1994).

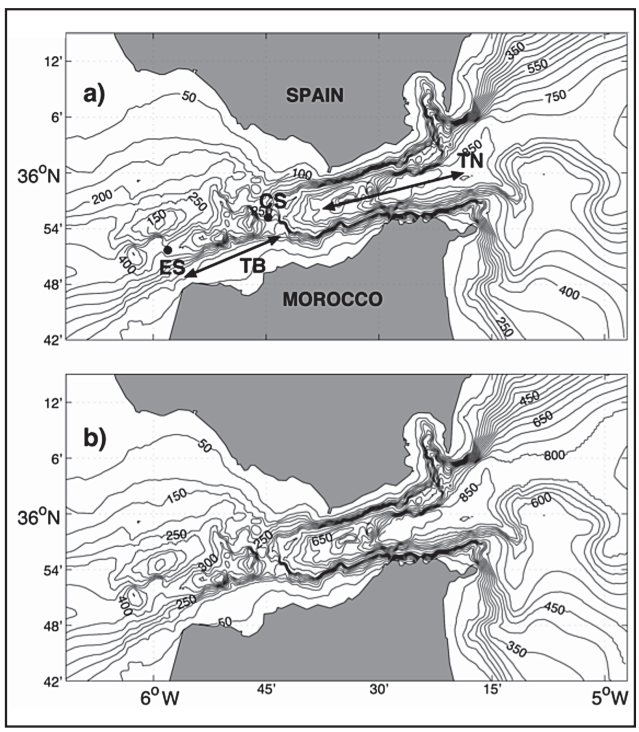

FIGURE 1 Bathymetry of the Strait of Gibraltar and location of Camarinal Sill CS, Espartel Sill ES, Tangier Basin TB and Tarifa Narrows TN

Upper panel: a) shows real bathymetry contours.
Lower panel: b) shows contours of the model bathymetry.

Source: images processed by the authors

In addition to observations, numerical models have turned out to be a very powerful tool for describing and interpreting the hydrodynamics of the SoG. Wang (1989) was probably the first author to numerically investigate the mean and tidal circulation in the Strait, followed later by the more recent works of Izquierdo et al. (2001), and Sannino et al. (2002, 2004, 2007), focusing more specifically on internal hydraulics processes.

As LAIWs have spatial scale of the order of 1 km and are highly non-linear and dispersive, a fine grid resolution together with the rejection of the hydrostatic assumption for the pressure field are crucial factors for modeling their generation and propagation. Although the generation mechanism of LAIWs in the SoG is generally understood, there are still some elements which deserve to be explored. Among the main features still not deeply investigated are the sensitivity of the generation process to the neap-spring cycle and the role of transversal (cross Strait) effects that take place during the propagation of the LAIWs in the Strait due to the three-dimensional variability of the bottom topography and lateral boundaries (Vlasenko et al. (2009)).

In this paper we numerically investigate the generation and evolution of LAIWs in the SoG without imposing any of the main simplifications used in previous numerical studies: the model is three-dimensional, fully nonlinear and non-hydrostatic. It is forced by a realistic barotropic tide covering the neap-spring cycle, and takes into account the underlying two-way exchange flow which represents the mean circulation of the Strait.

Model Setup

The simulation described in this paper was performed using the Massachusetts Institute of Technology general circulation model (MITgcm) The MITgcm solves the fully nonlinear, non-hydrostatic incompressible Navier-Stokes equations under the Boussinesq approximation with a spatial finite-volume discretization on a curvilinear computational grid. The model, described by Marshall et al. (1997a, b), implements the non-linear implicit free surface solution and partial step topography.

The model domain was discretized by a non-uniform curvilinear orthogonal grid of 1440x210 points extend-

ing in longitude from 6.3°W to 4.78°W. Spatial resolution along the axis of the Strait ranges between 46-63 m in the CS area and mesh size is always less than 70 m at the center of the domain. Across the Strait resolution is in the range 175-220 m near CS and less than 340 m in the middle of the Strait. Along the vertical axis, in order to capture the gradients at the pycnocline, the water column is discretized by 53 z-levels with a thickness of 7.5 m in the upper 300 m, increasing towards the bottom to a maximum of 105 m for the last 13 levels. Seafloor elevation in the model was calculated by merging the ETOPO2 bathymetry (U.S. Department of Commerce and NOAA/NGDC, 2001) with a high resolution bathymetry nautical chart (Figure 1b).

Temperature and salinity in the model domain were initialized using the climatologic Medar-MedAtlas Database (MEDAR Group, 2002) for the month of April. The average two-way exchange, which does not include tidal forcing, was obtained by laterally driving the model with the mean baroclinic velocities and tracers extracted from the intermediate resolution model developed by Sannino et al. (2009). At the open boundaries wave reflections are minimized by introducing a Newtonian relaxation term in the tracer equations and adopting the flow relaxation scheme proposed by Carter and Merrifield (2007) for the velocity field.

The model was initially brought to a quasi-steady two-way exchange by running for 11 days a simulation without tidal forcing. Tidal forcing due to the main diurnal (O1, K1) and semi-diurnal (M2, S2) components was subsequently introduced by prescribing barotropic tidal currents extracted from the intermediate resolution model at the open boundaries. A stable time periodic configuration was reached by running the simulation for 8 more days. Starting from this state the actual numerical experiment was carried out by running the model for a full tropical month (about 30 days).

Due to the great computational effort required, the model has been run on the CRESCO supercomputer installed at ENEA, C.R. Portici.

Models Results

The numerical experiment allowed us to distinguish between three types of tidal cycles in terms of the characteristics of the baroclinic response at CS, which depends upon the strength of the barotropic tidal forcing. The intensity of the tidal forcing can be quantified by the maximum barotropic tidal velocity during the tidal cycle (Umax) over Camarinal crest (Figure 1), or equivalently by the maximum value of the internal Froude number, where c is the propagation velocity of the first baroclinic mode, provided by the boundary value problem (Baines, 1998):

$$[(U(z)-c)\eta_z]_z+N^2(z)\eta = 0$$

$$\eta(-H) = \eta(0) = 0$$

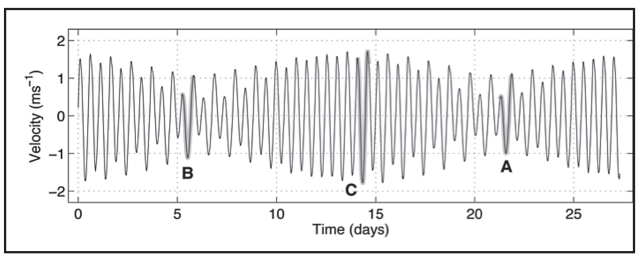

FIGURE 2 Barotropic tidal velocity over Camarinal Sill obtained during the numerical simulation.
Tidal cycles discussed in the paper are indicated in thick gray line.
Source: images processed by the authors

Here U(z) is the background velocity profile, N(z) the buoyancy frequency, and the vertical isopycnal displacement. Resolution of the equation taking profiles corresponding to the steady two-way exchange flow at Camarinal gives a propagation velocity for the first baroclinic mode ms^{-1} (the higher eingevalue).

Results reveal that the baroclinic response consists in the generation of a long-wavelength internal wave (internal tide). For Froude numbers above this limit, LAIWs developing at CS take the form of internal bores and solitary waves. Here we focus on this upper range, which in turn can be split into two regimes depending on the characteristics of the generated internal waves. In analyzing the overall generation process of LAIWs we consider the wave fields along the central axis of the Strait.

Moderate Forcing

We consider tidal cycles of moderate forcing those in which 1.1<Fr< 1.75. Let us analyze the baroclinic response at the lower bound of this range. Figure 3 shows the evolution of density and velocity fields in

the surroundings of Camarinal area at different times during tidal cycle A (Figure 2, Fr = 1.16). In panel 3a tidal outflow is increasing and approaching its maximum value during the tidal cycle (see velocity indicated at the low right corner of the panel), as a result an internal bore develops at the eastern edge of Camarinal crest, where the barotropic flow undergoes a strong spatial acceleration and the flow becomes critical. Downstream another hydraulic transition occurs at the western flank of the sills, as proved by the presence of an internal hydraulic jump surrounded by areas of intense water mixing. Such areas are highlighted in Figure 3 as gray contours enclosing regions of the water column where the Richardson number

$$\frac{Ri = N^2}{(u_z+v_z)^2} < 0{,}25$$

and shear instability may develop. Near the hydraulic jump instabilities arise as a result of a flow bifurcation where Mediterranean water spatially accelerates downslope Camarinal. Further away, shear instabilities occur all over Tanger basin at the interface between Atlantic and Mediterranean waters due to the strong shear current. Vertical expansion of the isopycnals observed in Tanger Basin attests that intense water mixing and entrainment take place in the area. This is even more evident 40 minutes later, when tidal currents reach their maximum value (Figure 3b). At this stage the Mediterranean layer undergoes an important temporal acceleration (compare arrows in panels 3a-b), as a consequence the shear current becomes stronger and the dynamic in the basin more turbulent. Multiple unsteady perturbations of the density field attest this fact. Among these perturbations a single coherent structure representing a second mode baroclinic wave can be identified at the lee side of CS (Figures 3b-c). This wave could be recognized 4 hours before, although not very clearly, in the configuration depicted in panel 3a (see counter-phase isopycnal displacements around x = -5 km). This structure is trapped at the lee side of the Camarinal where barotropic flow is weaker than the one over the top of the sill. At this particular location it encounters critical conditions due to its lower phase speed, estimated in 0.56 ms−1, and grows more and more in amplitude as it gains energy from the background barotropic flow. A similar scenario is found by Vazquez et al. (2006).

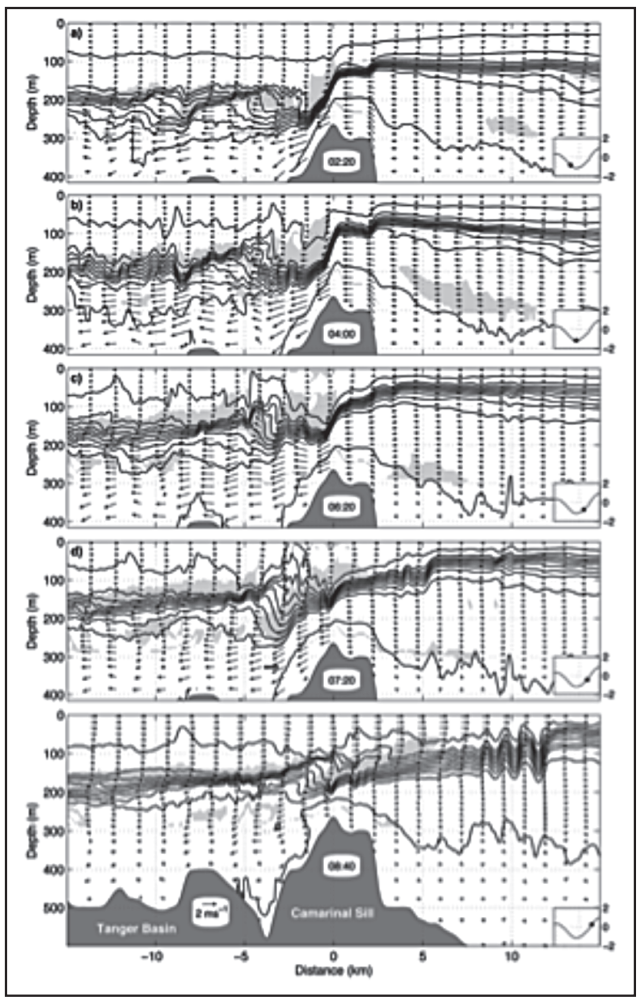

FIGURE 3 Evolution of the potential density field along central axis of the Strait during tidal cycle A (see Figures 2)

Isopynals shown are = 26.80, 27.05,..., 28.80, 29.02. Time origin is taken at the beginning of the tidal outflow. Arrows indicate the current velocity. Gray contours are zones in which the Richardson number Ri < 1/4, where shear instabilities may develop. The value of barotropic tidal current velocity (depth-averaged velocity) over Camarinal Sill is shown at the low right corner of panels.

Source: images processed by the authors

The first-mode baroclinic bore formed upstream starts propagating immediately after barotropic current relaxes over the sill (Figure 3c). When doing so, it disintegrates into a series of internal solitary waves due to nonlinear and dispersive effects (Figures 3c-e). The second mode begins its propagation about one hour

later (Figure 3d) falling behind the leading first-mode wave packet due to its lower velocity. It is worth to mention that the second baroclinic mode propagates in a very sheared (unstable, see Figure 3e) area sustaining strong viscous dissipation along its way. Further on, the second baroclinic mode stops being the dominant wave structure (Figure 3d) and vanishes in the eastern part of the Strait.

Immediately after its release, the upstream internal bore starts self-disintegrating into a series of solitary waves (Figure 3d). During this intermediate stage of the bore evolution both nonlinear and dispersive effects are amplified, determining a steepening of the leading edge of the bore, and the formation of a wiggling wave tail. The balance between the competing nonlinear and dispersive effects leads to the formation of a rank ordered solitary wave packet with amplitudes ranging between 30 and 70 meters (See Figure 3e). When this wave packet is 10 km away from CS, the second mode baroclinic bore is progressing just over Camarinal, considerably weakened in hardly 1.5 hours (compare panel 3d-3e). In fact, at a later stage this second mode bore almost vanishes in Tarifa narrows. This fact is attributed to the strong shear it encounters along its way (see panel 3e), which activates instabilities and viscous damping.

Strong Forcing

The generation characteristics of LAIWs under strong barotropic forcing, in the limit Fr > 1.75, are examined in this section. Forcing of this strength is found in some tidal cycles during spring tides, as in cycle C (Figure 2). In this extreme limit the upstream internal bore does not remain over the sill as in the previous case. Instead, as barotropic current increases, the internal bore is swept down at the lee side of CS (Figure 4a-b), where it merges with the second hydraulic jump located downstream (Figure 4c). At the same time an additional hydraulic jump forms over the secondary sill west of Camarinal (400 m depth, x=-7 km), where several unsteady LAIWs are trapped (Figure 4c-d). Immediately after its formation the leading bore (hydraulic jump) gradually disintegrates into a couple of large amplitude solitary waves, a process which takes place after its definitive release to the Alboran Sea (Figure 4c-e). On the other hand, the system of short waves trapped downstream the secondary sill, very un-

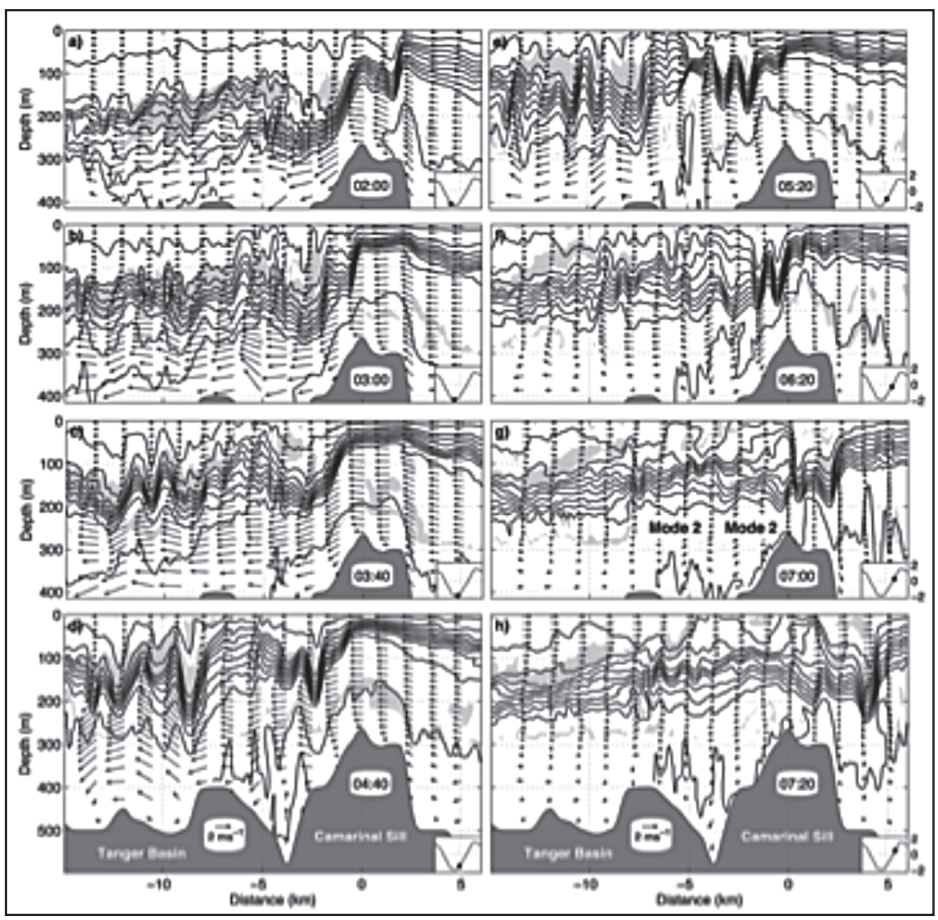

FIGURE 4 Same as Figure 3 for the tidal cycle C (Figure 2)
Source: images processed by the authors

steady, progressively degrades as the barotropic current slackens. In fact, only a weak track of these waves can be found at the time the leading waves pass over Camarinal crest (Figure 4f-g), and tidal flow reverses. This behavior is explained by the characteristic of the area where this system of waves develops, very sheared and unstable. On the contrary, where the leading hydraulic jump is located the velocity field looks quite barotropic and stable with the exception of vertical shear induced by positive strong surface currents associated to internal waves.

Stable waves eventually arise in the basin when tidal currents fade and shear relax, as the second mode baroclinic wave shown in Figure 4f at x = −6 km. This perturbation consolidates in the subsequent hour as a coherent structure slowly progressing eastwards (Figure 4g). This is not the only second mode wave at that time in the basin, a similar structure is generated in the front as a result of the interaction between the leading first mode LAIW and the bottom topography of CS (see Figures 4f-h). Such process of energy cascade from first to secondary internal modes driven by wave-topography interactions is discussed in detail in Vlasenko and Hutter (2001), and evidence of it has been reported in some other places of the World Ocean Vlasenko and Alpers (2005).

After passing CS the leading system of waves evolves into a rank ordered packet of solitary waves with amplitudes ranging between 90 and 160 m (Figure 5) shaped by nonlinear dispersion (larger waves propagate faster), unexpectedly losing its regular structure in the course of time. This process was recently described by Vlasenko et al. (2009), who explained it in terms of transversal effects: LAIWs interact with the lateral boundaries where they partially break while some energy is reflected and in turn absorbed by the waves propagating behind which grow in amplitude.

The very last remark concerns the formation of the hydraulic jump at the eastern flank of CS with a maximum ebb tide (Figures 5b-d). In agreement with satellite observations, the simulation does not reveal any LAIW formation from this pycnocline depression in any of the tidal cycles. Excluding the bathymetric effects, the underlying two-way exchange flow is the main responsible for this asymmetry in the generation of LAIWs with the ebb and flood tide. This is more evident when analyzing the numerical results of Vazquez et al. (2006), who did not include the mean flow of the Strait of Gibraltar in their model and found westwards propagating solitary waves. During the ebb tide the tidal flow cancels the mean velocity of the lower layer at CS, and increases the velocity of the upper layer. This leads to a very sheared velocity profile with the generation of areas of shear instability over CS and Tanger basin which likely inhibit the formation of stable propagating waves.

Conclusions

Generation and evolution of LAIWs in the Strait of Gibraltar is numerically investigated by means of a high resolution, three-dimensional, fully nonlinear, non-hydrostatic model. Results of the one-month numerical experiment allowed us to distinguish between

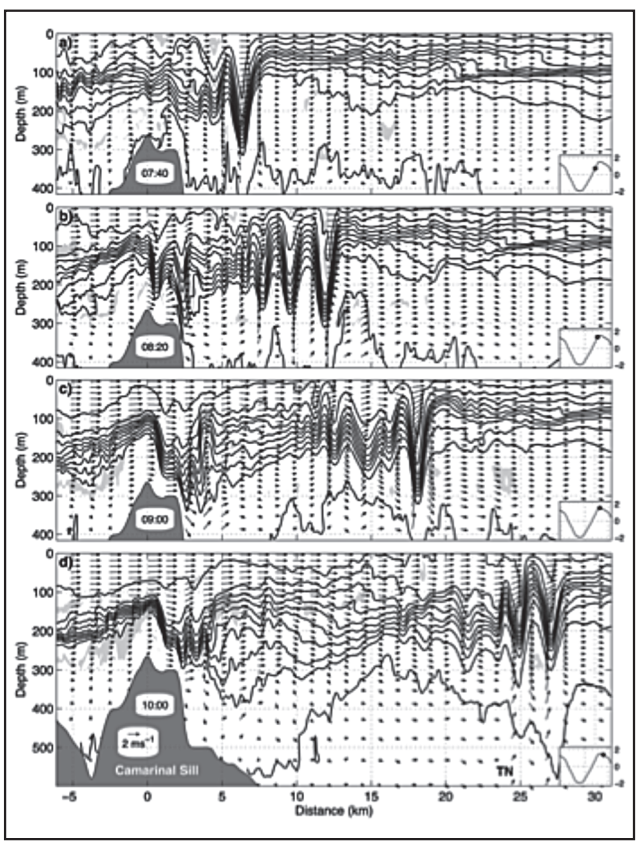

FIGURE 5 Temporal extension of Figure 4
Source: images processed by the authors

two types of tidal cycles depending on the nature of the internal wave field generated in CS area and related to the strength of the barotropic forcing over Camarinal crest.

Under moderated forcing (1.1 < Fr < 1.75, Figures 3) the scenario is fairly similar to that described in Vazquez et al. (2006). An internal bore is generated over CS just where the barotropic flow undergoes a strong spatial acceleration. The bore remains trapped by the flow, progressively growing in amplitude until the background current slackens and it finally disintegrates into a series of solitary waves propagating in the Alboran Sea. Downstream the flow bifurcates in a stagnant surface layer and fast downslope undercurrent, where another hydraulic jump is formed surrounded by a region where shear instabilities and mixing take place. At the same time, further downstream a second mode LAIW evolves and is released later than the first mode internal bore due to its lower phase velocity.

Under strong forcing (approximately beyond Fr > 1.75, Figures 4-5) the upstream internal bore is swept downstream where it merges with the hydraulic jump located at the lee side of the sill. The unstable region is shifted further downstream of Tanger basin, beyond secondary bathymetric features where another hydraulic transition occurs and very unsteady LAIWs remain trapped. In the course of time the hydraulic jump located at the lee side of the sill evolves into solitary waves eventually travelling eastwards when the background flow slackens. LAIWs trapped downstream, however, vanish at this stage when they cannot extract any more energy from the barotropic flow because of shear instabilities, and only secondary modes generated in the basin in a subsequent stage can finally propagate to the Alboran Sea. Generation of secondary waves as a result of the interaction of solitary waves with CS when those pass over the sill also occurs.

Bibliografia

[1] Baines, P.G., (1998), *Topographic Effects in Stratified Flows*. Cambridge University Press.

[2] Bryden, H.L., and T.H. Kinder (1991), *Steady two-layer exchange through the Strait of Gibraltar*. Deep-Sea Res I, 38, S1, S445-S463.

[3] Candela, J., C. Winant, and H.L. Bryden, (1989), *Meteorologically forced subinertial flows through the Strait of Gibraltar*. J. Geophys. Res. 94, 12667-12674.

[4] Carter, G.S. and M.A. Merrield, (2007), *Open boundary conditions for regional tidal simulations*. Ocean Modelling, 18, 194-209.

[5] Farmer, D.M. and L. Armi, (1988), *The flow of Mediterranean Water through the Strait of Gibraltar*, and Armi, L. and D.M. Farmer, (1988), *The flow of Atlantic Water through the Strait of Gibraltar*, Prog. Oceanogr., 21(1), 1-105.

[6] Izquierdo, A., L. Tejedor, D. Sein, J. Backhaus, P. Brandt, A. Rubino, and B. Kagan (2001). *Control variability and internal bore evolution in the Strait of Gibraltar: a 2-D two-layer model study*. Estuarine Coastal Shelf Sci., 53, 637-651.

[7] Marshall, J., C. Hill, L. Perelman, and A. Adcroft, (1997) *Hydrostatic, quasihydrostatic, and nonhydrostatic ocean modeling*. J. Geophysical Res., 102(C3), 5733-5752.

[8] Marshall, J., A. Adcroft, C. Hill, L. Perelman, and C. Heisey, (1997) *A finite-volume, incompressible Navier Stokes model for studies of the ocean on parallel computers*. J. Geophysical Res., 102(C3), 5753-5766.

[9] Richez, C., (1994). *Airborne synthetic aperture radar tracking of internal waves in the Strait of Gibraltar*. Prog. Oceanogr. 33, 93-159.

[10] Sannino, G., Bargagli, A., Artale, V., 2002. *Numerical modeling of the mean exchange through the strait of Gibraltar*. J. Geophys. Res. 107 (8), 9 1-24.

[11] Sannino, G., Bargagli, A., Artale, V., 2004. *Numerical modeling of the semidiurnal tidal exchange through the strait of Gibraltar*. J. Geophys. Res. 109, C05011, doi:10.1029/2003JC002057.

[12] Sannino, G., Carillo, A., Artale, V., 2007. *Three-layer view of transports and hydraulics in the strait of Gibraltar: A three-dimensional model study*. J. Geophys. Res. 112, C03010, doi:10.1029/2006JC003717.

[13] Sannino, G., Pratt, L., Carillo, A., 2009. *Hydraulic Criticality of the Exchange Flow through the Strait of Gibraltar*. J. Phys. Oceanogr. 39 (11), 2779-2799.

[14] Vazquez, A., N. Stashchuk, V. Vlasenko, M. Bruno, A. Izquierdo, and P. C. Gallacher (2006), *Evidence of multimodal structure of the baroclinic tide in the Strait of Gibraltar*, Geophys. Res. Lett., 33, L17605, doi:10.1029/2006GL026806.

[15] Vazquez, A., M. Bruno, A. Izquierdo, D. Macias, and A. Ruiz-Canavate (2008). *Meteorologically forced subinertial flows and internal wave generation at the main sill of the Strait of Gibraltar*, Deep Sea Res. I, 55, 1277-1283.

[16] Vlasenko, V.I. and K. Hutter (2001), *Generation of second mode solitary waves by the interaction of a first mode soliton with a sill*, Nonlin. Processes Geophys., 8, 223-239.

[17] Vlasenko, V., and W. Alpers (2005), *Generation of secondary internal waves by the interaction of an internal solitary wave with an underwater bank*, J. Geophys. Res., 110, C02019, doi:10.1029/2004JC002467.

[18] Vlasenko, V., J.C. Sanchez Garrido, N. Stashchuk, J. Garcia Lafuente, and M. Losada (2009), *Three-Dimensional Evolution of Large-Amplitude Internal Waves in the Strait of Gibraltar*. J. Phys. Oceanogr., 39, 22302246.

[19] Wang, D., (1989), *Model of mean and tidal flows in the Strait of Gibraltar*, Deep-Sea Res. 36, 1535–1548.